Progress In Electromagnetics Research C, Vol. 122, 183–198, 2022

Wireless Power Supply Voltage Regulation Control of Implantable Devices Based on Primary Side MPC

Weihua Chen*, Jiawei Song, and Xiaoheng Yan

Abstract—The wireless power transfer (WPT) system for implantable medical devices has the problem that the output voltage is difficult to adjust stably in real time without using additional composite compensation topology and dual-side communication. A primary side control method of WPT system based on a phase shifted full bridge inverter and continuous control set model predictive control (MPC) is proposed. First, series-series (SS) structure parameters and fundamental harmonic analysis (FHA) are used to derive the estimated value of the output voltage and establish the output voltage prediction model of the system. Then, to obtain the best response of the system, the optimization problem in the controller is transformed into the problem of solving the minimum value of the cost function, and the optimal control variable is obtained limited below the gradient descent method. Simulated and experimental results show that the control system works at a frequency of 200 kHz to realize real-time voltage adjustment, and the steady-state error is within 2%. Compared with the traditional method, the method reduces the adjustment time by 5–10 ms, and voltage overshoot is reduced by 5.3–6.7% when interference factors are dealt with such as load interference and mutual inductance. The proposed method improves the performance of SS compensated WPT systems to be more suitable for the applications that require compact and light weight receiver. It provides an effective method to realize the real-time regulation of the system output voltage.

1. INTRODUCTION

In recent years, Magnetic Coupled Resonant Wireless Power Transfer (MCR-WPT) has been widely used in solving the power supply problem of implantable medical equipment due to its long transmission distance and high transmission efficiency [1]. However, MCR-WPT system is susceptible to the change of mutual inductance and load, resulting in instability of the output voltage. The relatively large fluctuation of output power prolongs the charging time and increases the psychological burden of patients [2–4]. To overcome the above shortcomings, new control strategies need to be proposed. Existing primary side control methods [5–7] usually rely on wireless communication modules. The voltage signal is passed from the secondary side to the primary side as a reference signal for the controller. Then, by adjusting the duty cycle of the DC-DC converter, or the phase shift angle, or the operating frequency of the full-bridge inverter, real-time adjustment of the system voltage is achieved. Although many papers have made detailed introduction of these methods, there are still some problems to be solved [8–10]: additional hardware and software cost caused by the wireless communication module, and the delay of the feedback information which leads to the real-time control being infeasible. Wireless communication is not suitable in some special conditions, such as in the human body. Some scholars have analyzed the primary side control method based on parameter estimation for the above problems. In [11], a load and mutual inductance identification method for parallel compensation IPT system

Received 7 June 2022, Accepted 3 August 2022, Scheduled 11 August 2022

* Corresponding author: Weihua Chen (fxlgd@163.com).

The authors are with the Faculty of Electrical and Control Engineering, Liaoning Technical University, Huludao 125105, Liaoning, China.

based on primary side detection information is proposed. From the established identification model, the identification result is obtained, but it increased the control complexity and size of the WPT system. In [12], a multi-parameter estimation algorithm is proposed to identify the load resistance and mutual inductance from the transmitter information, and more accurate estimated parameters are obtained. However, it also increased the difficulty of the controller design. In [13], a load identification method is proposed to calculate active power using reflected impedance theory, and the estimated value and PI control are combined to achieve output voltage regulation. In [14], a primary-side control method for WPT is proposed based on a phase-shifted full-bridge inverter. An equation for estimating charging current and voltage using only primary side parameters is deduced, and voltage regulation is realized by combining with a double closed-loop PI controller. Most of the above methods use PI controllers, but the gain link is necessary for these methods, increasing the controlling difficulty. Existing research on primary side control methods without dual-side communication is still insufficient. Model Predictive Controller (MPC) [15–19] can precisely control the system according to the mathematical model of the control object to improve the dynamic response of the system. In addition, it is suitable for nonlinear systems that do not need to adjust the controller gain. In [20], MPC method is adopted to ensure the stable operation of the WPT system in the case of rapid changes in the coupling coefficient of the system. In [21], an MPC is designed to improve the dynamic response of the output voltage. In [22], an output voltage regulation method based on finite control set model predictive control (FCS-MPC) is proposed for an MC-WPT system. It has the advantages of intuitive concept, no need for modulator, and fast dynamic response. However, dual-side communication is still required, and there is a certain delay.

Therefore, in order to reduce the cost, volume, and complexity by removing the wireless communication module in the implantable medical equipment, this paper proposes a new primary side MPC method without double-ended communication, which realizes the real-time voltage adjustment of the WPT after SS compensation. An equation for estimating the output voltage only using the primary side parameters is derived as the reference value of the controller. At the same time, in order to enable the system to achieve stable output quickly during external disturbances such as load or parameter change, an MPC is designed. By controlling the full-bridge inverter, the control system can adjust the stable output voltage in real time and reduce the charging time of the device. An effective method is provided for realizing the real-time stable regulation of the output voltage of the implanted WPT system.

2. SYSTEM STRUCTURE AND THEORETICAL ANALYSIS

The basic principle of the primary side MPC strategy proposed in this paper is shown in Figure 1. The full-bridge inverter and full-bridge rectifier consist of four MOSFETs ($Q_1 \sim Q_4$) and four diodes ($D_1 \sim D_4$). Capacitive filter C_f ensures stable charging voltage. L_p, L_s, C_p, and C_s constitute SS compensation. The mutual inductance between the coils is M. U_{in} is the system input DC voltage. u_{AB} is the output voltage of the inverter. The resonant currents flowing through the coil are i_P and i_s, respectively. u_{CD} and R_{CD} are the input voltage and input resistance of the full-bridge rectifier. The output current and voltage are I_0 and U_0. R_L is the equivalent load resistance. The estimated output voltage from the primary side parameters is sent to the controller without using dual-side communication. Combined with the MPC controller, voltage regulation is achieved by regulating the full-bridge inverter.

2.1. Inverting and Rectifying Models

The output voltage of the full-bridge inverter circuit is a square wave u_{AB}. Fourier series decomposition is performed on u_{AB}. Considering that it is symmetrical about the origin, it does not contain DC components and cosine components only contains sine components. The Fourier series of the leaf transform is:

$$u_{AB} = \frac{4}{\pi} U_{in} \sum_{n=0}^{+\infty} \frac{(-1)^k}{2k+1} \sin\left(\frac{(2k+1)\,\pi}{2}\right) \sin\left((2k+1)\,\omega \mathrm{t}\right) \tag{1}$$

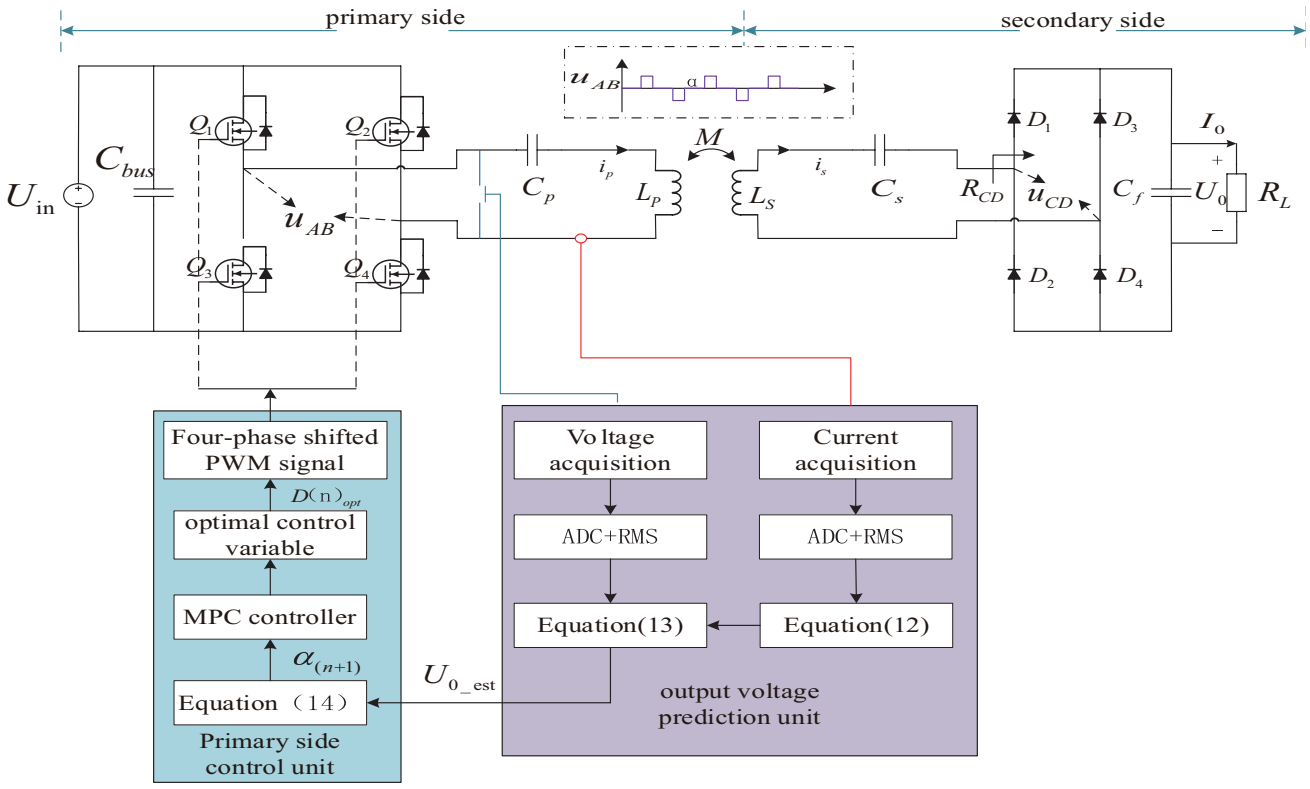

Figure 1. Schematic diagram of the control strategy.

The root mean square (RMS) value U_{AB} expression of the inverter voltage can thus be written as (2), where α is the phase shift angle.

$$U_{AB} = \frac{2\sqrt{2}}{\pi} \cos\frac{\alpha}{2} U_{in} \tag{2}$$

By adjusting α, U_{AB} is adjusted, and I_0 and U_0 are also adjusted. Therefore, a phase-shifted H-bridge inverter is employed to implement the proposed control method. With Fundamental Harmonic Analysis (FHA) and the law of conservation of energy, the relationship between the rectification and filter circuits at the receiving end is deduced, including the relationship between U_{CD} and I_s (RMS value) and R_{CD}, U_0, I_0, R_L

$$U_{CD} = \frac{2\sqrt{2}}{\pi} U_0, \quad I_0 = \frac{2\sqrt{2}}{\pi} I_s, \quad R_{CD} = \frac{8}{\pi^2} R_L \tag{3}$$

2.2. Mutual Inductance Model

In Figure 2, Z_{in} is the equivalent input impedance of the system; R_p and R_s are the internal resistances of the primary and secondary coils of the system, respectively. It can be derived from Kirchhoff's Voltage Law that

$$\begin{bmatrix} Z_P & j\omega M \\ j\omega M & Z_S \end{bmatrix} \begin{bmatrix} \dot{I}_p \\ \dot{I}_s \end{bmatrix} = \begin{bmatrix} \dot{U}_{AB} \\ 0 \end{bmatrix} \tag{4}$$

In Equation (4), both the primary side impedance and the secondary side impedance of S-S compensation are expressed as

$$Z_p = R_p + j\left(\omega L_p - 1/\omega C_p\right), \quad Z_s = R_s + R_L + j\left(\omega L_s - 1/\omega C_s\right) \tag{5}$$

According to the principle of reflection impedance, the impedance Z_{RF} reflected from the secondary side to the primary side is:

$$Z_{RF} = \frac{(\omega M)^2}{R_L + j\left(\omega L_s - \dfrac{1}{\omega C_s}\right) + R_s} \tag{6}$$

The equivalent input impedance Z_{in} of the system is:

$$Z_{in} = R_P + j\left(\omega L_P - \frac{1}{\omega C_P}\right) + Z_{RF} \tag{7}$$

From Equations (4) and (5), the resonant currents on the primary and secondary sides are obtained

$$\begin{cases} \dot{I}_p = \dfrac{Z_s}{(\omega M)^2 + Z_p Z_s}\dot{U}_{AB} \\ \dot{I}_s = \dfrac{1}{j}\dfrac{(\omega M)}{(\omega M)^2 + Z_p Z_s}\dot{U}_{AB} \end{cases} \tag{8}$$

The analysis shows that changes in R_L affect I_p, and the relationship between I_p and I_0 or U_0 is deduced through (3), (5), and (8), which suggests that U_0 can be regulated by adjusting I_p even if R_L is not known. It satisfies the assumption that the primary side controller can regulate the output voltage without a dual-side communication.

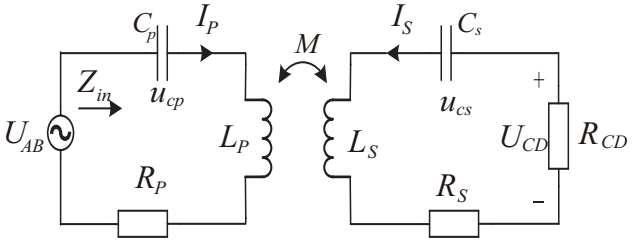

Figure 2. Equivalent mutual inductance model.

3. PRIMARY SIDE MPC CONTROLLER DESIGN

To mitigate the dynamic problem caused by the load and other changes in WPT system, MPC scheme is adopted in this paper. Figure 3 shows a schematic diagram of the MPC method. Based on the feedback

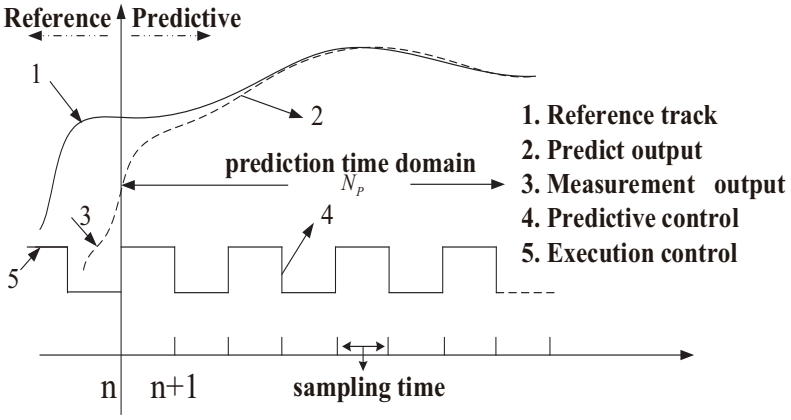

Figure 3. Schematic diagram of model predictive control.

of voltage $U_0(n)$, the controller uses a prediction model to predict the output voltage $U_0(n+1)$ for the next sampling period of all possible voltage pulse trains. Substitute $U_0(n+1)$ and its reference value U_{0_est} into the cost function for evaluation, and select the voltage pulse sequence that minimizes the cost function as the switching signal applied to the inverter for the next control cycle. By repeating this process continuously, scroll optimization is done to achieve fast tracking control of U_0. The proposed controller consists of three main parts: U_0 prediction model, cost function, and feedback correction, which are described in the following subsections.

3.1. Output Voltage Prediction

The battery can be seen as a variable load during charging, calculated by U_0/I_0. During the analysis of the load identification method, the battery is assumed to be a resistor. Neglecting secondary side losses, the power delivered to the battery is equal to the power consumed by the real part of Z_{in}. Active power P_1 is derived from Equation (7):

$$P_1 = I_P^2 Re\left(Z_{in}\right) \tag{9}$$

When the system works in the resonance state, the load R_L can be expressed as:

$$R_L = \frac{\pi^2}{8}\left[\frac{\left(\omega M\right)^2 I_p^2}{P_1 - R_p I_p^2} - R_s\right] \tag{10}$$

The controller and sensors can calculate and measure P_1 and I_p, and then obtain the estimated value of the load R_L. Further, the RMS value of the S-S compensation resonant current i_p is derived from (2)–(3) and (7)–(8).

$$I_p = \frac{2\sqrt{2}\left(\pi^2 R_s + 8R_L\right)}{\pi R_p\left(\pi^2 R_s + 8R_L\right) + \pi^3\left(\omega M\right)^2}\cos\frac{\alpha}{2}U_{in} \tag{11}$$

It can be seen from (11) that I_p is affected by the load R_L, while I_p is controlled by α. Then, the output voltage U_0 is controlled by controlling I_p. According to the analysis above, the output voltage estimation Equation (13) is obtained by combining Equations (10)–(12).

$$A = \sqrt{\left(\frac{1-\omega^2 C_s L_s}{\omega C_s}\right)^2 + \left(R_s + \frac{8}{\pi^2}R_L\right)^2}$$

$$I_0 = \frac{2\sqrt{2}I_p\omega M}{\pi * A} \tag{12}$$

$$U_{0\_est} = \frac{2\sqrt{2}I_p\omega M R_L}{\pi * A} \tag{13}$$

It can be seen from Equation (13) that I_p is a measurable variable on the primary side, which can realize primary side MPC proposed in this paper. The MATLAB simulation results are shown in Figure 4. As α increases, the resonant current I_p and output voltage U_0 decrease. Therefore, U_{0_est} is estimated as the reference voltage value of the MPC controller by using the primary side measurable P_1, I_p. Voltage regulation is then achieved by adjusting α.

In order to obtain the voltage prediction model, Equation (13) is discretized to obtain the output voltage $U_0(n+1)$ in the sampling period of the voltage pulse sequence in the prediction model:

$$U_0\left(n+1\right) = \frac{8R_L\omega M * U_{in}\cos\left(\dfrac{\alpha\left(n+1\right)}{2}\right)}{\pi^2\left(R_p + \dfrac{\omega^2 M^2}{R_s + \dfrac{8}{\pi^2}R_L}\right) * A} \tag{14}$$

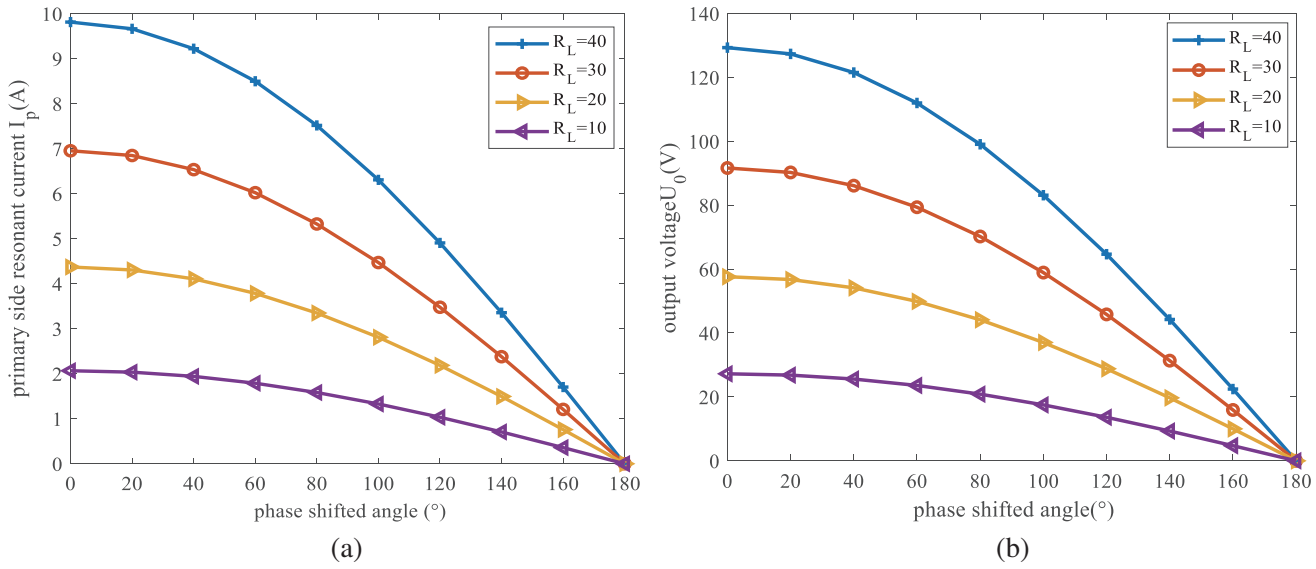

Figure 4. Phase shifted angle versus load resistance. (a) Primary side resonant current and (b) output voltage.

3.2. Cost Function

In order to minimize the output error and obtain the best response of the system. The cost function is used to reflect the core of the MPC objective, and the solution of the cost function at each control time is called a rolling optimization process. Generally, the tracking characteristics of the system output to the reference input and the constraints during the operation of the system should be taken into account when the cost function is designed. Therefore, the cost function of model predictive control in this paper is expressed in the following form:

$$J\left(N_P, N_C\right) = \sum_{i=k}^{N_P} \lambda\left(k\right)\left[U_0\left(n+k\right) - U_{set}\left(n+k\right)\right]^2 + \sum_{i=k}^{N_C} \delta\left(k\right)\left[\Delta D\left(n+k\right)\right]^2 \tag{15}$$

where N_P, N_C are the prediction range and control range of the controller; $U_0(n)$ and $U_{set}(n)$ are the model output value and the reference value; ΔD, $\lambda(k)$, $\delta(k)$, are the control variables and the two weighting factors. In this controller, to reduce the computational burden, the prediction range is limited to one step ($N_P = 1$). According to [23], this control range is suitable for voltage tracking in power electronic systems. The remaining parameters are selected as follows:

$$\begin{aligned} N_C &= 1 \\ J\left(N_P, N_C\right) &= \sum_{k=1}^{1}\left[U_0\left(n+k\right) - U_{set}\left(n+k\right)\right]^2 + \sum_{i=k}^{1} \delta\left(k\right)\left[\Delta D\left(n+k\right)\right]^2 \end{aligned} \tag{16}$$

To make the output curve meet the desired target and achieve the purpose of optimization, J is the cost function that needs to be minimized. Find the second derivative of (16):

$$\begin{cases} \dfrac{\partial J\left(N_P, N_C\right)}{\partial y_r} = 0 \\ \dfrac{\partial^2 J\left(N_P, N_C\right)}{\partial y_r^2} > 0 \end{cases} \tag{17}$$

The cost function has a minimum value, because the second derivative is positive. So the control problem is transformed into the problem of minimizing the cost function J under constraints, and the

optimal value of the control variable can be arranged in increments by Equation (14):

$$\alpha_{(n+1)} = 2\cos^{-1}\left[\frac{U_0\left(n+1\right)\pi^2\left(R_p + \dfrac{\omega^2 M^2}{R_s + \dfrac{8}{\pi^2}R_L}\right) * A}{8\omega M U_{in}}\right] \tag{18}$$

Optimize the solution to minimize the cost function J, and the optimal value of the phase shift angle $D(n)_{opt}$ can be obtained by solving the following process:

$$\begin{aligned} &D\left(n\right)_{opt} = \operatorname{argmin}\left(J\left(N_P, N_C\right)\right) \\ &0 \le \alpha_{(n)} \le \pi \\ &\Delta D\left(n\right) = \alpha_{(n)} - \alpha_{(n-1)} \end{aligned} \tag{19}$$

Equation (16) is a convex optimization problem, and the gradient descent method can be used to solve the optimal control variable value. The iterative equation of the gradient descent method is as follows:

$$D\left(n\right)_{opt} = D\left(n\right)_{opt} - L_r\frac{\partial J}{\partial D\left(n\right)} \tag{20}$$

In the equation, L_r is the learning rate of gradient descent, and $\partial J/\partial D(n)$ is the derivative of $D(n)$, thereby obtaining the optimal control variable $D(n)_{opt}$ for controlling the regulation voltage of the WPT system.

3.3. Feedback Correction

In order to ensure the accuracy of the prediction result, it is necessary to perform feedback correction on the output of the system. The calculation equation of feedback correction is as follows:

$$\begin{aligned} e\left(n-1\right) &= U_0\left(n-1\right) - U_{set}\left(n-1\right) \\ y_p\left(n\right) &= U_0\left(n\right) + L\left(e\left(n-1\right)\right) \end{aligned} \tag{21}$$

where $U_0(n-1)$ represents the predicted output at time $n-1$; $U_{set}(n-1)$ represents the actual sampling value of the system at time $n-1$; $e(n-1)$ is the error value; $y_p(n)$ is the actual predicted value of the system state prediction model at time n; and L is the feedback correction coefficient. Use this error information to predict future errors and use this to compensate for model-based predictions.

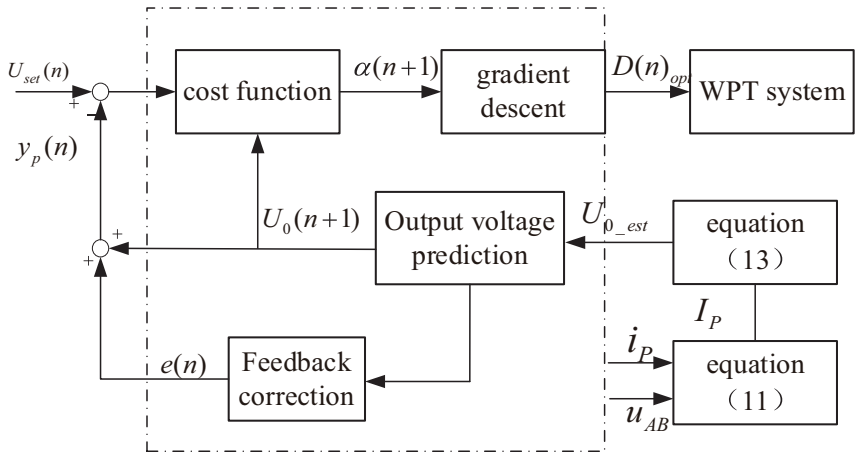

Figure 5. Primary side MPC block diagram.

The controller designed above is shown in Figure 5. The voltage and current are measured by the sensor. Substitute this into Equation (13) to estimate the output voltage. The estimated output voltage U_{o_est} is compared with the set reference value, and the obtained error is input to the MPC controller, and then the optimal control variable of the system can be calculated according to Equation (20) to adjust the output voltage of the system.

4. SIMULATION VERIFICATION

According to the previous analysis, the primary side MPC controller is designed, and the proposed control method is verified by MATLAB/Simulink. The simulation circuit model as shown in Figure 1 is built, and the control algorithm and the simulation model form a closed control loop to verify the effectiveness of the proposed method. At the same time, it is compared with the traditional control method PID control and MPC using bilateral communication, proving the superiority of the primary side MPC. Set the simulation parameter sampling time to 0.001 s, and the prediction range and control range values are both 1. The output voltage deviation has a weight of 0.9, and the incremental weight of $\cos(\alpha)$ is 0.1. The rest of the system simulation parameters are shown in Table 1.

Table 1. System parameter.

symbol	Parameter	Value
f	Rated system working frequency	200 kHz
L_P	Transmitter coil inductance	30 μH
R_P	Transmitter coil resistance	0.16 Ω
L_S	Receiver coil inductance	30 μH
R_S	Transmitter coil resistance	0.16 Ω
C_p	Compensation capacitor	21.109 nF
C_s	Compensation capacitor	21.109 nF
R_L	Equivalent load resistance	8-16 Ω
M	Rated mutual	7.52 μH
C_f	Filter capacitor	47 μH
U_X	Battery voltage range	15–25 V

According to the theoretical analysis in Section 3, the validity of the algorithm and the accuracy of the load estimation are verified. In Figures 6 and 7, the solid line is the setting curve, and the dashed line is the system output curve. Figure 6 shows the set and estimated load resistance values. R_L can track the set point well, and the maximum error is 1.9%. Figure 7 shows the tracking effect of the system output voltage. Except the deviation in the change stage of the set value, the voltage prediction value in the whole stage can better track the set value. The effectiveness of model predictive control in dealing with nonlinear and constrained systems is verified.

After the algorithm verification, the necessity of closed-loop control needs to be verified in the circuit. Configure the electrical parameters as shown in Table 1, and set the simulation time to 0.15 s. Set the reference voltage to 15 V, reduce the resistance value from 16 Ω to 8 Ω in 0.075 s, and compare and simulate with the traditional method. The simulation results are shown in Figure 8. Compared with the traditional control method, the adjustment speed of the primary side MPC scheme is faster and can reach the set value in 0.015 s, and when a disturbance occurs, the controller returns to the set value within 10 ms. The output of the device is stable at 15.09–15.23 V, and the steady-state error is 1.5%. Meanwhile, the output voltage under the traditional MPC and PID controllers has fluctuations of ±2.2% and ±3%. The method proposed has higher control precision and faster adjusting speed.

To verify the ability of the proposed control strategy to track the change of mutual inductance, the reference voltage is set to 15 V; the mutual inductance M is reduced from 7.52 μH to 4.72 μH in 0.075 s;

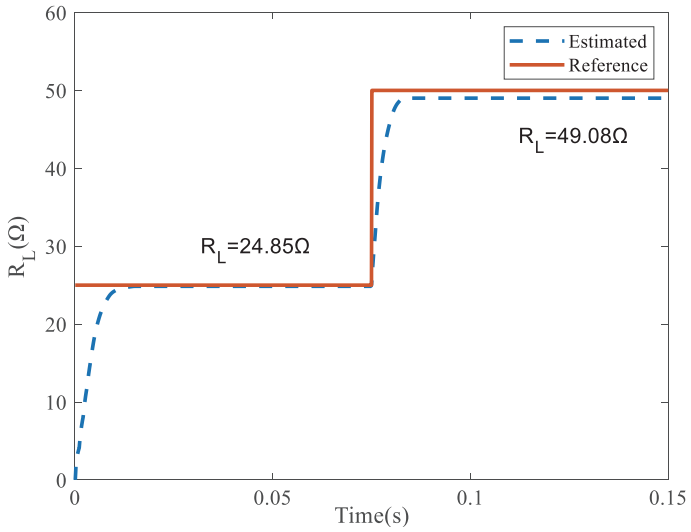

Figure 6. Equivalent load resistance estimation diagram.

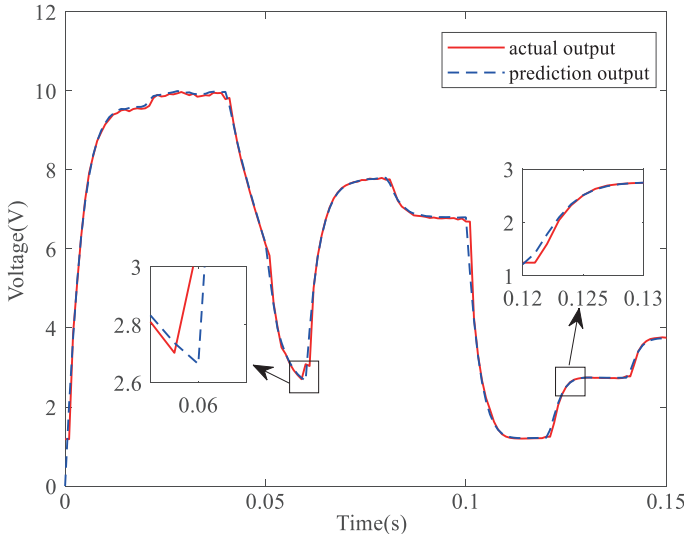

Figure 7. System output tracking diagram.

and the system dynamic performance simulation is carried out. The simulation results are shown in Figure 9. When the disturbance occurs, the voltage of the method proposed recovers to 14.76–14.92 V after a transient response of 12 ms. Under transient conditions, the voltage overshoot of the MPC scheme is lower than that of the PID controller due to inductance changes. All three methods have obvious fluctuations after stabilization among which the method in this paper has relatively small fluctuations. The controlling process of the proposed controller is significantly faster and smoother than traditional control strategies.

To verify the anti-parameter interference ability, the initial value is set to 21 V, and the reference value is changed to 15 V in 0.075 s. By changing the operating frequency to 100 kHz and 300 kHz, the remaining parameters are the same as in Table 1, and the anti-parameter interference characteristics of the system are observed to verify the robustness of the system. The simulation results are shown in Figure 10. From Figure 10(a), it can be seen that there is high frequency oscillation in the output voltage of the PID controller whose resonant frequency changes, and a stable output voltage cannot be maintained. It can be seen from Figure 10(b) that using the MPC controller, when the resonant

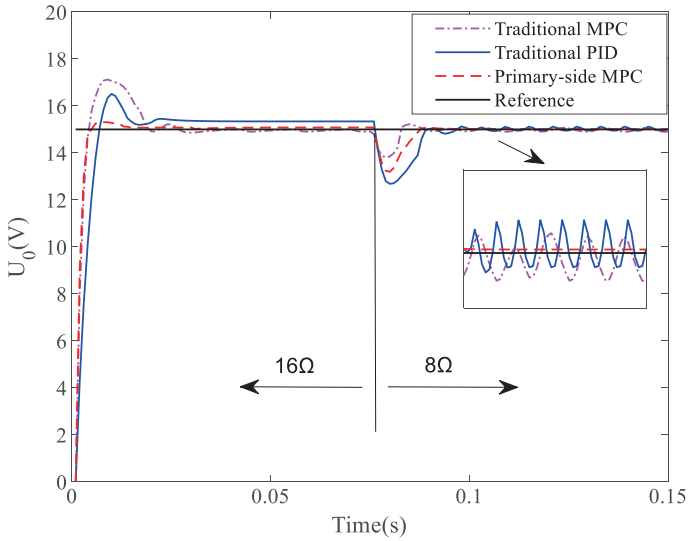

Figure 8. Load disturbance simulation result.

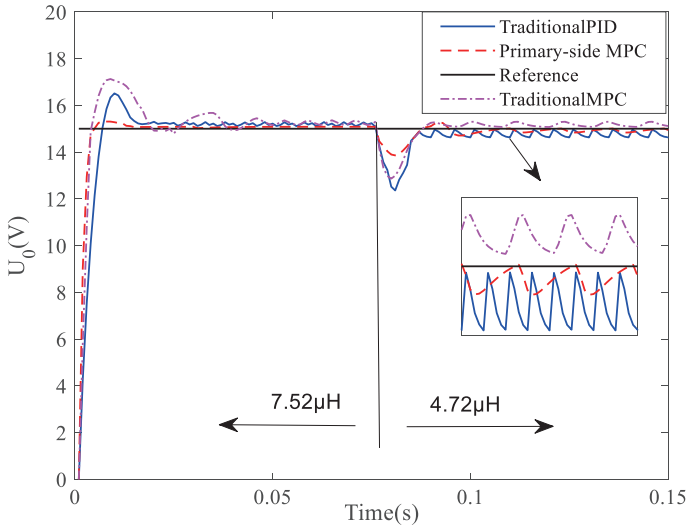

Figure 9. Mutual inductance disturbance simulation result.

frequency changes by 300 kHz and 100 kHz, the overshoot of the system becomes larger, and the output steady-state error is 4.7% and 3.5%, respectively. Compared with the PID controller, although the steady-state error of the controller increases when the system resonance parameters change, the control strategy of the proposed method still has a certain ability to adjust the output voltage.

5. EXPERIMENTAL STUDIES

The sampling frequency of the experimental prototype in this paper is 200 kHz. According to the experimental device of the corresponding implantable wireless power transmission system, the experimental circuit diagram is shown in Figure 11. The MPC is implemented with TMS32F334, inverter, and rectifier, using MOSFET (Infineon IRFP15N60L) and diode (Fairchild FFA60UP30DN), respectively. The selection of the size of the transmitting and receiving coils is $20 \times 20\,\text{mm}^2$, and the other parameters are shown in Table 1. To verify the effectiveness of the controller, the regulation ability and anti-disturbance ability of the system are respectively verified.

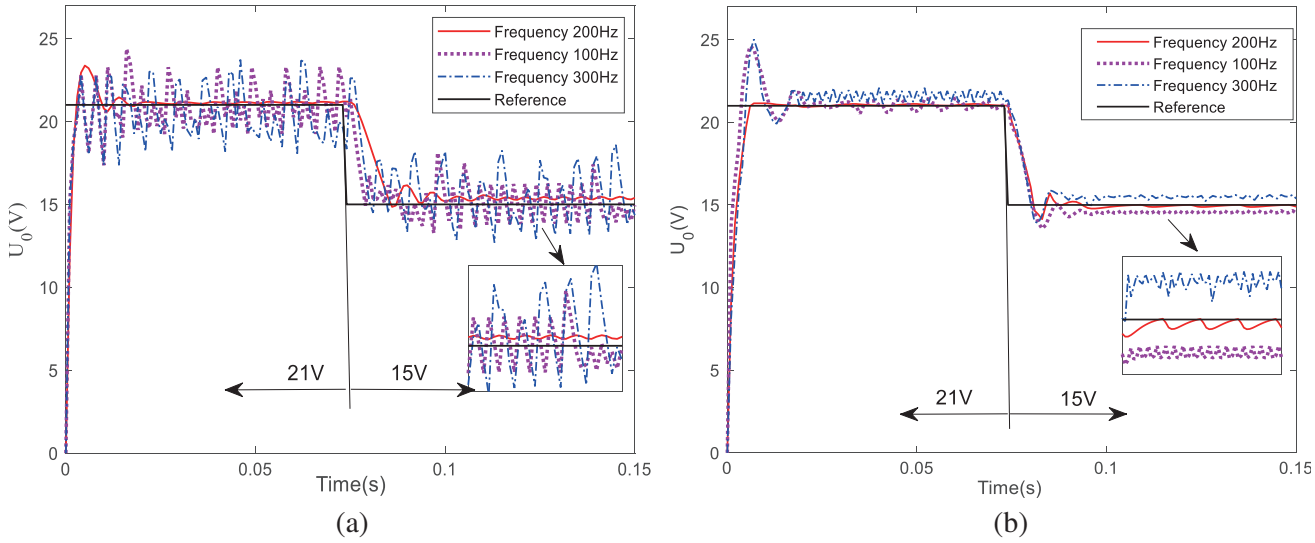

Figure 10. Simulation of system parameter changes, (a) PID, (b) primary side MPC.

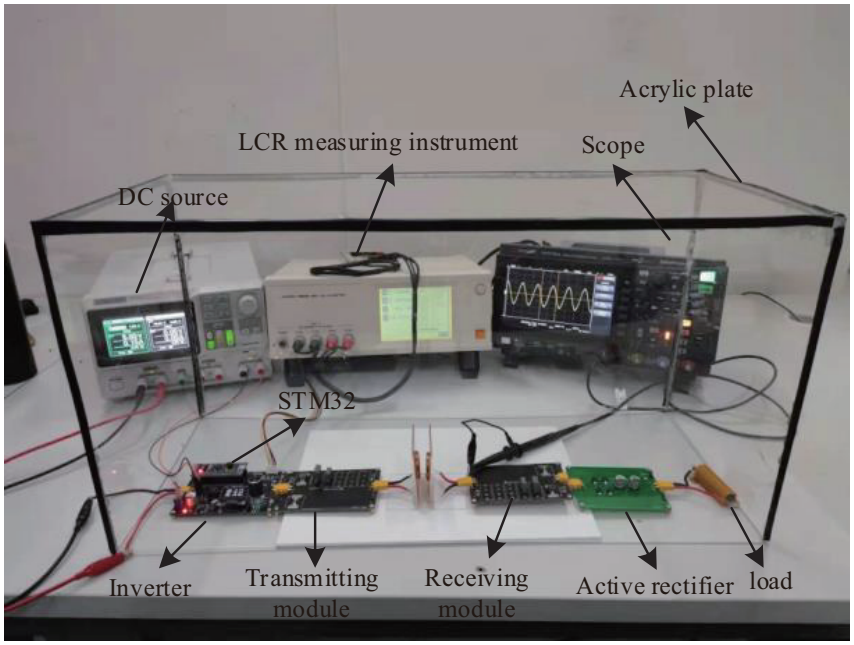

Figure 11. Experimental circuit.

5.1. Steady State Experiment

Figure 12 shows the steady-state working waveform of the method proposed in this paper. Under the condition that the load resistance is 16 Ω, and the input voltage is 5 V, the output voltage distribution of the inverter is observed. The waveform distribution is relatively regular, which proves the steady-state performance of the designed controller good.

During the steady state experiment, the estimated output voltage of the SS compensation controlled by the phase shift angle α was measured, and the results are plotted in Figure 13. As can be seen from the figure, the estimated output voltage is basically consistent with the measured value. The results

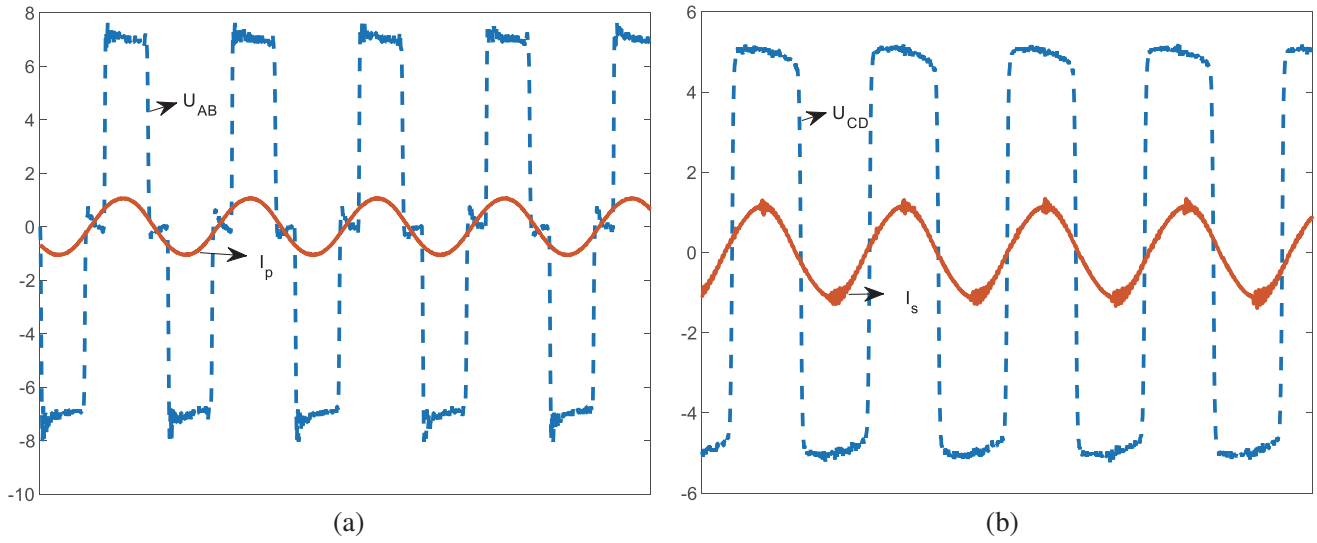

Figure 12. Steady-state working waveform, (a) primary side waveform, (b) secondary side waveform.

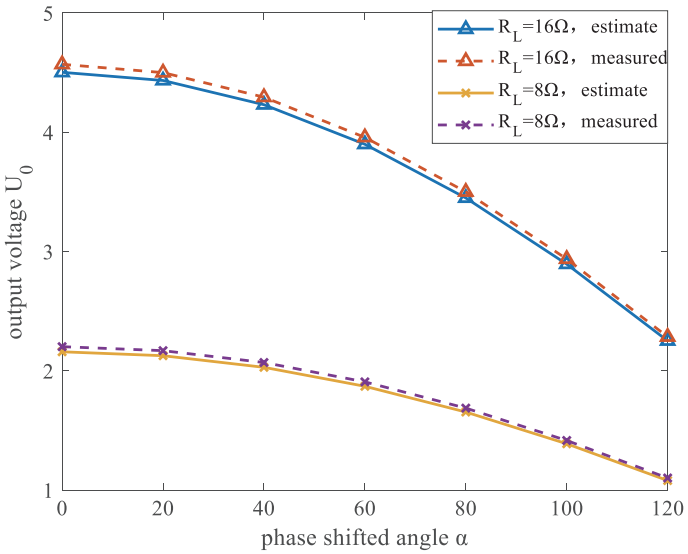

Figure 13. Controllability test experiment.

show that as the load resistance increases, the pass phase shift angle increases to maintain a constant output voltage. Among them, the estimation accuracy of U_0 is limited by the following factors: the measurement error of the sensor and calculation error of the controller. Nonetheless, both simulated and experimental results verify the feasibility of the primary-side control method.

5.2. Dynamic Experiment

In order to verify the dynamic performance of the proposed method, the output voltage is set to 10 V, and then the reference voltage is suddenly changed to 15 V. After that, the output voltage curve and inverter voltage curve are observed. It can be seen from Figure 14 that after the set voltage is changed to 15 V, the voltage regulation is completed within 0.03 s. It shows that the controller has a certain voltage regulation ability, and the steady-state error is 2.3%.

Under the MPC scheme and PID control scheme, the output voltage is set to 15 V and $R_L = 16\,\omega$.

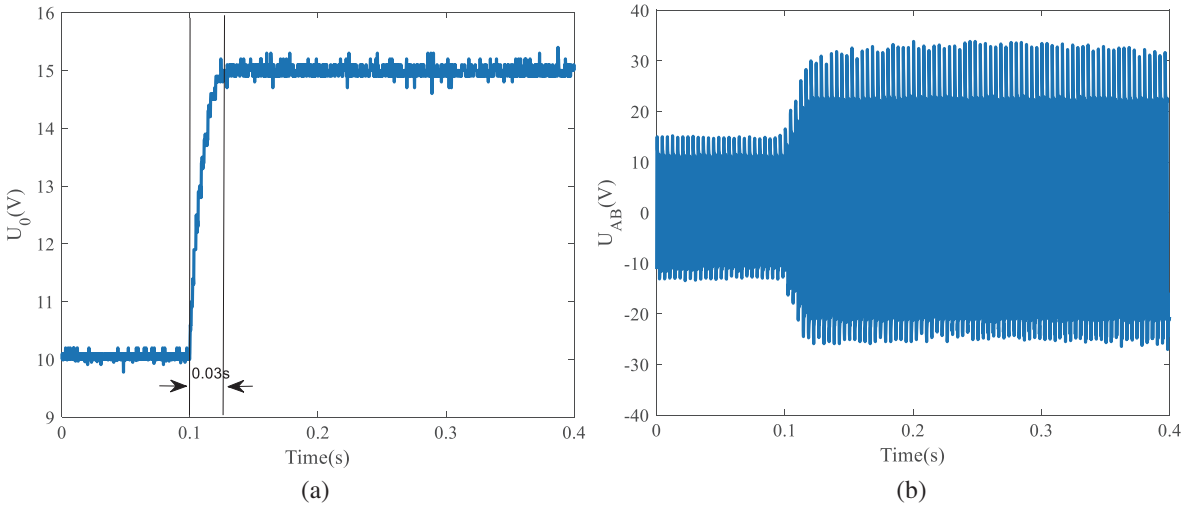

Figure 14. Experiment results of voltage regulation. (a) Output voltage curve. (b) Inverter voltage curve.

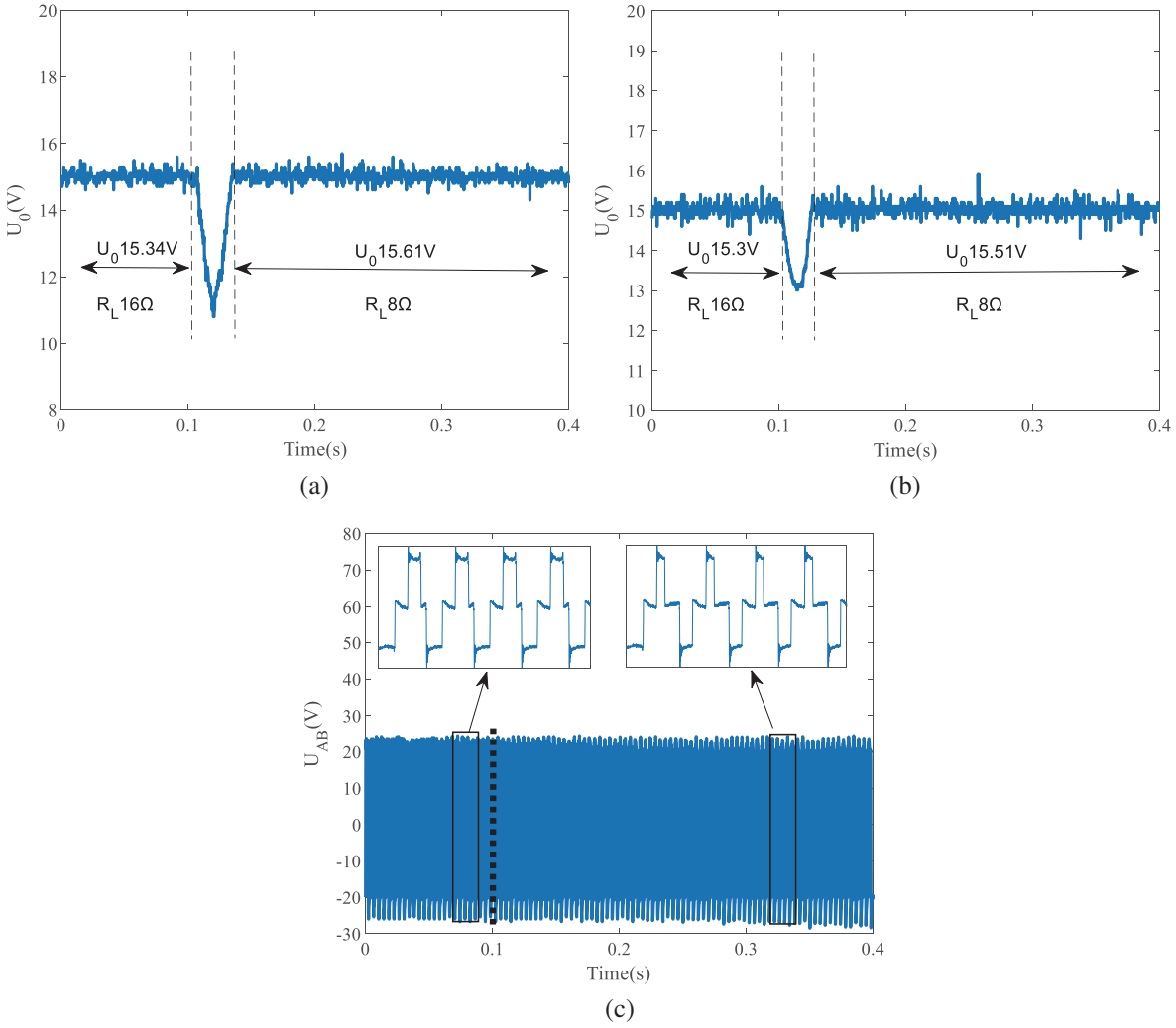

Figure 15. Experimental results of transient load changes, (a) PID output voltage, (b) primary side MPC output voltage, (c) inverter voltage curve.

Then change the load to 8 Ω, and observe the voltage output curve and the inverter output voltage curve. The experimental results are shown in Figure 15. After the system load becomes 8 Ω, the system output voltage is reduced, and it is restored to 15.51 V in a short time. The steady-state error is 3.4%. Compared to the PID solution, the overshoot of the method is lower. It shows that the system can cope with the effect of load disturbance on the voltage and can quickly stabilize the output voltage to the set value.

The output voltage is set to 15 V, and the mutual inductance of the coupling coil is 7.52 μH by testing in static state. The coil is then shifted laterally by 0.5 cm. The measured mutual inductance becomes 4.72 μH at this time. Observe the voltage output curves of the two control schemes and the inverter voltage curves. The experimental results are shown in Figure 16. When the mutual inductance decreases, the output voltage stabilizes to 15.2 V within 0.04 seconds, and the steady-state error is 1.3%. The steady-state error of the PID control method reaches 5.4%. It shows that the controller can cope with the influence of mutual inductance disturbance on the voltage.

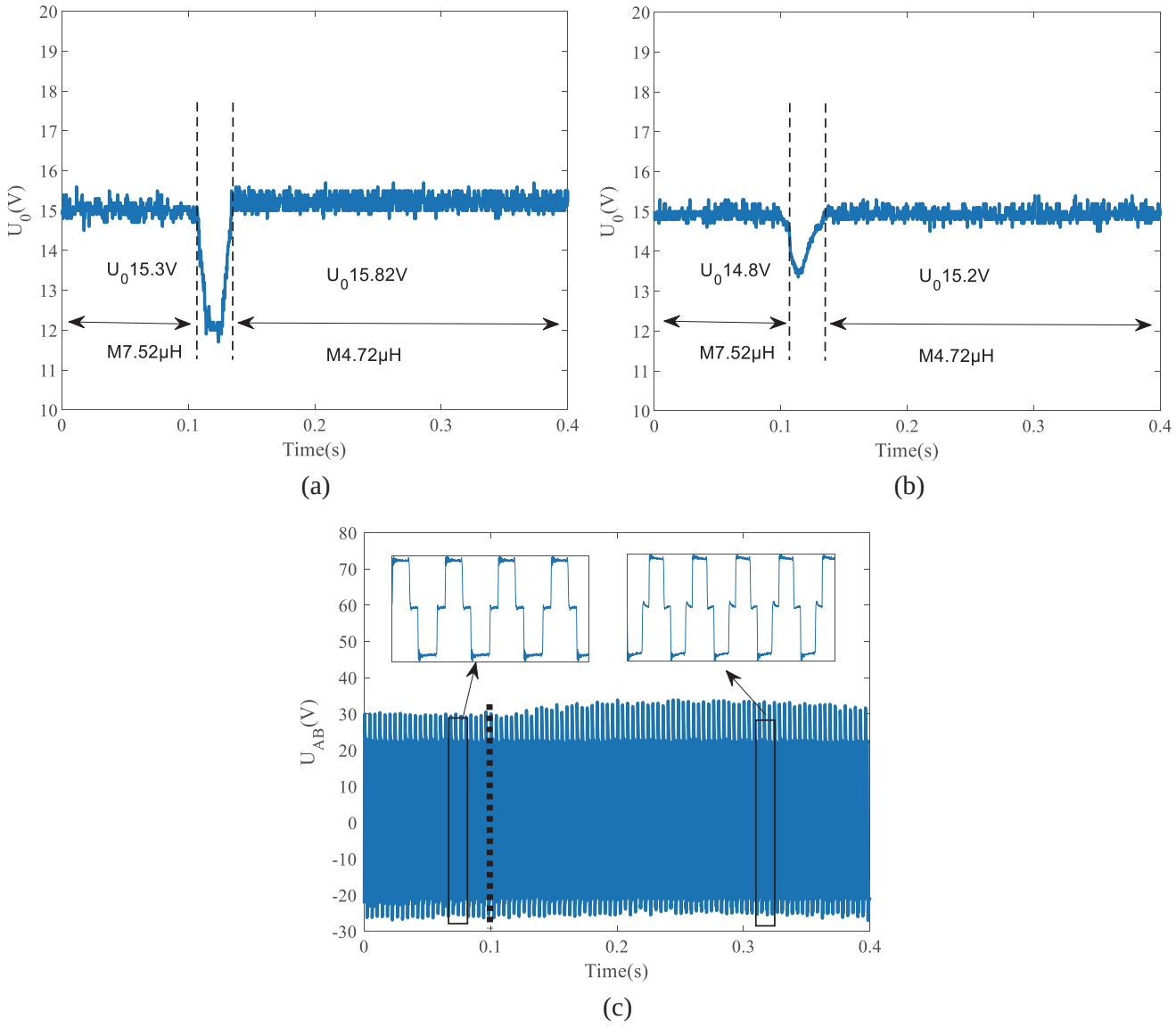

Figure 16. Experimental results of transient mutual inductance changes, (a) PID output voltage, (b) primary side MPC output voltage, (c) inverter voltage curve.

6. CONCLUSION

In this paper, a primary side MPC scheme is proposed for the real-time control of the output voltage of the implanted WPT system. The main research work includes:

(1) Taking the WPT system with S-S structure as an example, the output voltage is estimated by the primary side parameters without using dual-side communication of the system and fundamental harmonic analysis (FHA). The feasibility of primary-side model predictive control is analyzed.

(2) The output voltage prediction model of the system is established. In order to obtain the best response of the control system, the output optimization problem is converted into the problem of solving the minimum value of the cost function, and the gradient descent method is used to solve the optimal control variable. Compared with the traditional control method, the MPC controller based on this design does not need a modulator and has a fast and smooth dynamic transient response.

(3) Finally, the simulation and experimental verification of the controller are carried out. The results show that the proposed control strategy can track the reference voltage accurately and quickly. Compared with the traditional control method, the proposed method has good robustness to the load and mutual inductance disturbance of the system, and the steady-state error is within 2%. The adjustment time is reduced by 5–10 ms, and the voltage overshoot is reduced by 5.3–6.7%. The accuracy is improved by 1–3%, and the change in resonance parameters still has a certain adjustment ability, which provides an effective method for realizing the primary side control of the output voltage of the implanted WPT system.

REFERENCES

1. Qing, X. and Y. Su, "An overview of electric-filed coupling wireless power transfer technology," *Transactions of China Electrotechnical Society*, Vol. 36, No. 17, 3649–3663, 2021.
2. Martínez Rojas, J. A., J. L. Fernández, and R. Sánchez Montero, "Model-based systems engineering applied to trade-off analysis of wireless power transfer technologies for implanted biomedical microdevices," *Sensors*, Vol. 21, No. 9, 3201, 2021.
3. Fachrizal, R. and J. Munkhammar, "Improved photovoltaic self-consumption in residential buildings with distributed and centralized smart charging of electric vehicles," *Energies*, Vol. 13, No. 5, 1153, 2020.
4. Zhang, Z., H. Pang, A. Georgiadis, and C. Cecati, "Wireless power transfer — An overview," *IEEE Transactions on Industrial Electronics*, Vol. 66, No. 2, 1044–1058, 2018.
5. Ann, S. and B. K. Lee, "Analysis of impedance tuning control and synchronous switching technique for a semibridgeless active rectifier in inductive power transfer systems for electric vehicles," *IEEE Transactions on Power Electronics*, Vol. 36, No. 8, 8786–8798, 2021.
6. Yang, Y., W. Zhong, and S. Kiratipongvoot, "Dynamic improvement of series-series compensated wireless power transfer systems using discrete sliding mode control," *IEEE Transactions on Power Electronics*, Vol. 33, No. 7, 6351–6360, 2017.
7. Liu, G., J. Bai, and Y. Cui, "Frequency compound control method of MCR-WPT system," *Electric Machines and Control*, Vol. 24, No. 2, 9, 2020.
8. Miller, J. M., O. C. Onar, and M. Chinthavali, "Primary-side power flow control of wireless power transfer for electric vehicle charging," *IEEE Journal of Emerging and Selected Topics in Power Electronics*, Vol. 3, 147–162, March 2015.
9. Naghash, R., S. M. M. Alavi, and S. E. Afjei, "Robust control of wireless power transfer despite load and data communications uncertainties," *IEEE Journal of Emerging and Selected Topics in Power Electronics*, Vol. 9, No. 4, 4897–4905, 2020.
10. Hu, H., T. Cai, S. Duan, X. Zhang, J. Niu, and H. Feng, "An optimal variable frequency phase shift control strategy for ZVS operation within wide power range in IPT systems," *IEEE Transactions on Power Electronics*, Vol. 35, No. 5, 5517–5530, May 2020.
11. Su, Y.-G., "Load and mutual inductance identification from the primary side of inductive power transfer system with parallel-tuned secondary power pickup," *IEEE Transactions on Power Electronics*, Vol. 33, No. 11, 9952–9962, 2018.

12. Xiao, W., R. Shen, B. Zhang, D. Qiu, Y. Chen, and F. Xie, "Multiple parameters estimation based on transmitter side information in wireless power transfer system," *IEEE Access*, Vol. 7, 164835–164843, 2019.
13. Song, K., Z. Li, and J. Jiang, "Constant current/voltage charging operation for series-series and series-parallel compensated wireless power transfer systems employing primary-side controller," *IEEE Transactions on Power Electronics*, Vol. 33, No. 9, 8065–8080, 2017.
14. Li, Z., H. Liu, and Y. Tian, "Constant current/voltage charging for primary-side controlled wireless charging system without using dual-side communication," *IEEE Transactions on Power Electronics*, Vol. 36, No. 12, 13562–13577, 2021.
15. Wang, Y. and S. Boyd, "Fast model predictive control using online optimization," *IEEE Transactions on Control Systems Technology*, Vol. 18, No. 2, 267–278, 2009.
16. Urrutia, M., R. Cardenas, and J. C. Clare, "Circulating current control for the modular multilevel matrix converter based on model predictive control," *IEEE Journal of Emerging and Selected Topics in Power Electronics*, Vol. 9, No. 5, 6069–6085, 2021.
17. Xue, C., D. Zhou, and Y. Li, "Hybrid model predictive current and voltage control for LCL-filtered grid-connected inverter," *IEEE Journal of Emerging and Selected Topics in Power Electronics*, Vol. 9, No. 5, 5747–5760, 2021.
18. Chen, L., S. Shao, and Q. Xiao, "Model predictive control for dual-active-bridge converters supplying pulsed power loads in naval DC micro-grids," *IEEE Transactions on Power Electronics*, Vol. 35, No. 2, 1957–1966, 2019.
19. Zhou, Z., L. Zhang, Z. Liu, Q. Chen, R. Long, and H. Su, "Model predictive control for the receiving-side DC-DC converter of dynamic wireless power transfer," *IEEE Transactions on Power Electronics*, Vol. 35, No. 9, 8985–8997, 2020.
20. Shi, W., J. Deng, and Z. Wang, "The start-up dynamic analysis and one cycle control-PD control combined strategy for primary-side controlled wireless power transfer system," *IEEE Access*, Vol. 6, 14439–14450, 2018.
21. Liu, S., R. Mai, L. Zhou, Y. Li, J. Hu, Z. He, Z. Yan, and S. Wang, "Dynamic improvement of inductive power transfer systems with maximum energy efficiency tracking using model predictive control: Analysis and experimental verification," *IEEE Transactions on Power Electronics*, Vol. 35, No. 12, 12752–12764, 2020.
22. Qi, C., Z. Lang, and L. Su, "Finite-control-set model predictive control for a wireless power transfer system," *2019 IEEE International Symposium on Predictive Control of Electrical Drives and Power Electronics (PRECEDE)*, IEEE, 2019.
23. Garayalde, E., I. Aizpuru, and U. Iraola, "Finite control set MPC vs continuous control set MPC performance comparison for synchronous buck converter control in energy storage application," *2019 International Conference on Clean Electrical Power (ICCEP)*, 2019.